forests

MDPI

Article

Highly Mechanical Strength, Flexible and Stretchable Wood-Based Elastomers without Chemical Cross-Linking

Yongyue Zhang [1], Jiayao Li [1], Yun Lu [2] and Jiangtao Shi [1,3,*]

[1] Department of Wood Science and Engineering, College of Materials Science and Engineering, Nanjing Forestry University, Nanjing 210037, China; 18195486182@163.com (Y.Z.); lijiayao@njfu.edu.cn (J.L.)
[2] Research Institute of Wood Industry, Chinese Academy of Forestry, Beijing 100091, China; y.lu@caf.ac.cn
[3] Co-Innovation Center of Efficient Processing and Utilization of Forest Resources, Nanjing Forestry University, Nanjing 210037, China
* Correspondence: shijt@njfu.edu.cn

Abstract: Wood exhibits a limited elastic deformation capacity under external forces due to its small range of elastic limit, which restricts its widespread use as an elastic material. This study presents the development of a stretchable wood-based elastomer (SWE) that is highly mechanical and flexible, achieved without the use of chemical cross-linking. Balsa wood was utilized as a raw material, which was chemically pretreated to remove the majority of the lignin and create a more abundant pore structure, while exposing the active hydroxyl groups on the cellulose surface. The polyvinyl alcohol (PVA) solution was impregnated into delignified wood, resulting in the formation of a cross-linked structure through multiple freeze–thaw cycles. After eight cycles, the tensile strength in the longitudinal direction reached up to 25.68 MPa with a strain of ~463%. This excellent mechanical strength is superior to that of most wood-based elastomers reported to date. The SWE can also perform complex deformations such as winding and knotting, and SWE soaked in salt solution exhibits excellent sensing characteristics and can be used to detect human finger bending. Stretchable wood-based elastomers with high mechanical strength and toughness have potential future applications in biomedicine, flexible electronics, and other fields.

Keywords: polymer cross-linking; anisotropic structure

Citation: Zhang, Y.; Li, J.; Lu, Y.; Shi, J. Highly Mechanical Strength, Flexible and Stretchable Wood-Based Elastomers without Chemical Cross-Linking. *Forests* **2024**, *15*, 836. https://doi.org/10.3390/f15050836

Academic Editor: Alain Cloutier

Received: 17 April 2024
Revised: 2 May 2024
Accepted: 8 May 2024
Published: 10 May 2024

1. Introduction

Natural wood, with its small strain limit in the elastic range (~10%), has long been used as an engineering material such as beams and posts in timber-framed buildings or as a rigid material such as furniture, flooring, doors, and windows [1,2]. However, as a biomaterial that has evolved over millions of years, wood has developed a structural basis for responding to environmental stimuli and is a "smart material" that responds and adapts to its environment [3–5]. Although it exhibits some elastic deformation when subjected to external forces, its elastic limit range is relatively small, which limits its use as an elastic material [6,7]. Research on the structural control of wood to prepare elastic materials is limited. If the elastic properties of wood can be accurately regulated, it can be used as a high-performance green material in various fields including machinery, automobiles, sports and leisure, aerospace, home packaging, and other applications [8–10].

The elasticity of wood is greatly limited by its structure and composition. Macroscopically, wood has a complex cellular structure arranged in different directions to form an interwoven network that is susceptible to damage from stress concentration during the tensile process; at the molecular level, the lignin content of wood is positively correlated with cell wall rigidity, and the thermoplastic behavior of lignin is not conducive to the elastic deformation of wood [11–13]. Consequently, one of the most effective methods for the preparation of elastic materials from wood is the removal of lignin.

Balsa wood, which is produced in tropical America, is one of the lightest woods in the world. It is characterized by low density, high porosity, and rapid growth. Its superior axial stiffness, strength, and energy absorption make it one of the most attractive core materials [14,15]. Due to its low lignin content and rich pore structure, balsa is often used in the construction of wood-based elastomers. For example, Gao et al. used balsa wood as a raw material, hollowed out the wood ray tissue by the chemical cropping strategy, and obtained a superhydrophobic wood-based elastomer by chemical heat treatment [16]. Wang et al. chemically delignified and silylated balsa wood to obtain wood-based elastomers with high elasticity [17]. Song et al. obtained highly elastic wood-based elastic sensors from balsa wood by delignification treatment and MXene modification [18]. However, the elastic deformation ability of elastic wood is limited because it is inflexible and cannot be stretched. This limits its application in fields such as biomedical and flexible electronics. Therefore, it is important to develop wood-based elastic materials with stretchable properties.

In elastomers, cross-linking and entanglement between long-chain molecules can confer excellent tensile properties to the material, which provides new ideas for the preparation of flexible wood with tensile properties [19–21]. In recent works, flexible hydrogel materials based on wood can be produced by incorporating a network of polymer molecules into the wood fiber backbone [22,23]. For example, Dong et al. constructed a wood-based composite gel sensor by introducing PAM into the delignified lignin skeleton [24]; Wang et al. constructed composite wood-based gels using gelatin [25]; and Shen et al. utilized ionic liquid impregnation to obtain wood/polyionic liquid (WA/PIL) hydrogels [26]. However, the elastic tensile properties of natural wood are affected by its anisotropic structure, which has been overlooked in this process, and the three-dimensional network structure formed by the polymer molecular chains and the fiber skeleton in the wood is too weak to withstand higher stresses and larger strains, so there is a need for the further development of tougher wood-based elastic materials.

Herein, we have prepared a high mechanical strength, high flexibility, and stretchable wood elastomer through delignification treatment and polymer impregnation crosslinking. The removal of lignin can effectively expose highly active hydroxyl groups on cellulose molecular chains and form rich pore structures. Physical freezing and thawing can facilitate the formation of a stable cross-linking structure between the polyvinyl alcohol solution and the lignocellulosic fiber skeleton [27,28]. To explore the potential applications of this material, we proceeded to combine SWE with salt solutions, thus obtaining wood-based anisotropic elastomers (E-SWE) with conductivity. The directional arrangement of channel structures within the lignocellulosic framework can be exploited for ion transport, thereby conferring an excellent sensing performance for E-SWE. Compared to traditional fossil-based elastomers (rubber, polyurethane, polydimethylsiloxane), SWE is expected to become a new generation of biomass elastomers due to its simple preparation process, excellent performance, and environmental friendliness based on natural wood.

2. Materials and Methods

2.1. Materials

Balsa wood (*Ochroma pyramidale*, from South America, density~0.1 gcm^3) was cut into slices along its growth direction with the dimensions of 60 × 20 × 2 mm^3 (longitudinal × radial × tangential). Polyvinyl alcohol (PVA), sodium hydroxide (NaOH), sodium chlorite ($NaClO_2$), and glacial acetic acid were purchased from Nanjing Aladdin Biological Technology Co. Ltd. (Nanjing, China).

2.2. Delignification of the Balsa Wood

Balsa wood was immersed in a 6 wt% NaOH solution for 6 h at 90 °C in a water bath. The pretreated wood was washed 3~5 times with deionized water, and then the pretreated wood was delignified with 3 wt%$NaClO_2$ solution (pH~4.6 adjusted with acetic acid). The treatment time was about 6~8 h at 80 °C [29,30]. The obtained delignified wood samples were washed 3~5 times with deionized water and then freeze-dried.

2.3. Preparation of Super Stretched Wood Based Elastic Materials

The hydrogel solutions were first prepared as follows. Dissolve the PVA powder in deionized water at 95 °C and stir continuously with a magnetic stirrer to prepare PVA solutions with concentrations of 5% wt, 10% wt, and 15% wt. The PVA solution was poured into the delignified wood sample and vacuum impregnated at 200 Pa, with the vacuum being released at 30-min intervals to allow the hydrogel solution to fill the wood structure. This process was repeated three to four times. The impregnated samples were frozen in an ultra-low temperature refrigerator at a temperature of −60 °C for a period of one hour. Thereafter, the frozen samples were thawed naturally at room temperature for a period of two hours until they were completely thawed. The freeze–thaw process was repeated six to eight times in order to obtain stretchable wood-based elastomers (Figure 1). E-SWE with conductive properties was obtained by impregnating SWE into a salt (NaCl) solution for 24 h.

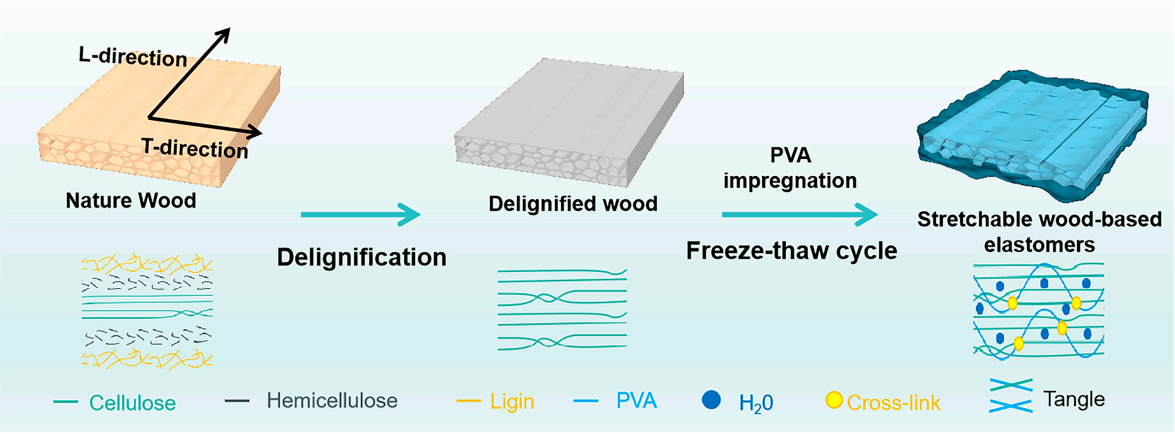

Figure 1. Construction method and mechanism of SWE.

2.4. Characterization

2.4.1. Morphology

Field emission scanning electron microscopy was used to observe the microscopic morphology of the cross section and chord section of natural wood and prepared SWE, respectively. The test voltage was 4 KV.

2.4.2. X-ray Diffraction Measurement

The cellulose crystal structure of the SWE was characterized using X-ray diffraction (Bruker D2 Phaser, Karlsruhe, Germany) with a scanning range of 5 °to 90 °(2θ); the speed was 2 s per degree. The crystallinity of the wood samples was calculated according to the Segal method. The crystallinity index (CrI) was determined according to Equation (1), where I_{200} is the maximum intensity of the 200 lattice diffraction around 22°, and I_{am} is the intensity of the amorphous diffraction at 18°.

$$CrI = \frac{I_{200} - I_{am}}{I_{200}} \times 100 \quad (1)$$

2.4.3. Small-Angle X-ray Scattering Measurement

Small-angle X-ray scattering (SAXS) measurements were performed at an X-ray wavelength (λ) of 0.154 nm, and the sample-to-detector distance was set to 1045 mm (Xeuss 2.0, Grenoble, France).

2.4.4. Fourier Transform Infrared (FTIR) Characterization

FTIR spectra were recorded in the range of 500−4000 cm^{-1} using a Nicolet iS10 FTIR spectrometer (Thermo Scientific Nicolet iS20, Waltham, MA, YSA).

2.4.5. Chemical Composition Analysis

Composition analysis of the wood samples was carried out according to the NREL (National Renewable Energy Laboratory, Golden, CO, USA) standard procedure.

2.4.6. Tensile Test

The tensile tests were performed on a universal material-testing machine (KXWW-01C, Chengde, China) utilizing a 100 N load cell at a crosshead speed of 5 mm/min. All specimens had a size of 30 mm × 5 mm with a thickness of around 1 mm.

2.4.7. Sensor Performance

An electrochemical workstation (CHI760E, Beijing Huake Putian Technology Co. Ltd., Beijing, China) was used to detect the resistance change of E-SWE. The AC voltage of the test resistor was 0.1 V, and the AC frequency was 1000 Hz. According to the resistance change of the hydrogel during the test, the resistance change rate trend of the entire process was calculated. $\Delta R/R_0 = (R - R_0)/R_0 \times 100\%$ (R_0 is the initial resistance during no-change operation during the test, R is the real-time resistance during the test).

The experimental data were analyzed using Excel (Microsoft Office Home and Student 2019) and Origin (OriginPro 2021).

3. Results and Discussion

3.1. The Physical Properties of SWE

The construction of the SWE was accomplished through a simple chemical pretreatment and physical freeze–thaw process. Various cells (wood fibers, rays, and conduits) constitute the anisotropic structure of natural wood. The fibers are oriented along the direction of growth for wood in the L-direction and perpendicular to the fiber direction in the T-direction. (Figure 1). In the cross-section shown in Figure 2a, honeycomb wood fibers were interlocked with each other, while the ray tissue was horizontally aligned along the radial direction [31]. In the delignification process, most of the lignin can be extracted in situ by pretreatment of the wood using NaOH solution, followed by the further removal of residual lignin using $NaClO_2$ solution (pH~4.6) to obtain white wood (Figure 2e) [32,33]. With the removal of lignin, the ray structure in natural wood was destroyed and replaced by a large cleavage structure (Figure 2f,g). Some of the cell wall structures in the cross-section were disrupted, resulting in a more porous and less dense channel structure. As a result of these treatments, the cellulose fibers exposed many highly reactive hydroxyl groups. However, the mechanical strength of the wood was weakened.

To reconstruct the loose and porous structure of delignified wood, filling the internal nanochannels with polymers is the preferred strategy. Therefore, biodegradable PVA (a commonly used polymer) was introduced into the system [34,35]. Polyvinyl alcohol, which contains abundant hydroxyl groups, can effectively reconstruct wood by forming hydrogen bonds with cellulose fibers. In our process, delignified wood was immersed in the PVA solution and vacuum impregnation was used to achieve complete penetration. The samples were frozen at −20 °C for 6 h, followed by gelation. This process was repeated 6 to 8 times. During the freezing process, the ice crystals will phase-separate from PVA and keep squeezing the PVA molecular chains and cellulose molecular chains, which is similar to a continuous forging process. By continuously repeating this process, the pore structure of the wood in the chordal section is basically covered (Figure 2j), and the interwoven PVA network structure is formed within the wood fiber channels in the transverse section (Figure 2k–l) [27,28]. This indicates that PVA formed a stable cross-linking structure with the wood fiber backbone.

SAXS is a powerful technique for characterizing the cell wall structure without affecting the internal structure [36]. Figure 3 shows the SAXS 2D scattering images of natural wood and SWE similarly presenting an elliptical shape, showing the oriented arrangement of cellulose nanofibrils (CNFs). The similar CNF orientation indicates that the wood retained its anisotropic structure after crosslinking by PVA impregnation. We then probed the

nanostructural changes of SWE using SAXS. The 1D maps derived from the 2D SAXS model were fitted, as shown in Figure 3a,b. The interfiber correlation length (d) was calculated from the peak centers of the Gaussian fits. In natural wood, the original fibers were densely arranged in a hemicellulose–lignin matrix with a fiber spacing of ≈3.04 nm, which was similar to the values reported in other studies (~3–4 nm) [37]. The SWE fibers obtained after polymer impregnation and crosslinking had a spacing of ≈7.34 nm; the increase in fiber spacing was conducive to the penetration of long-chain polymers into the fibers and the formation of a denser crosslinking network structure with the fibers, which could more easily withstand a greater amount of stress and strain.

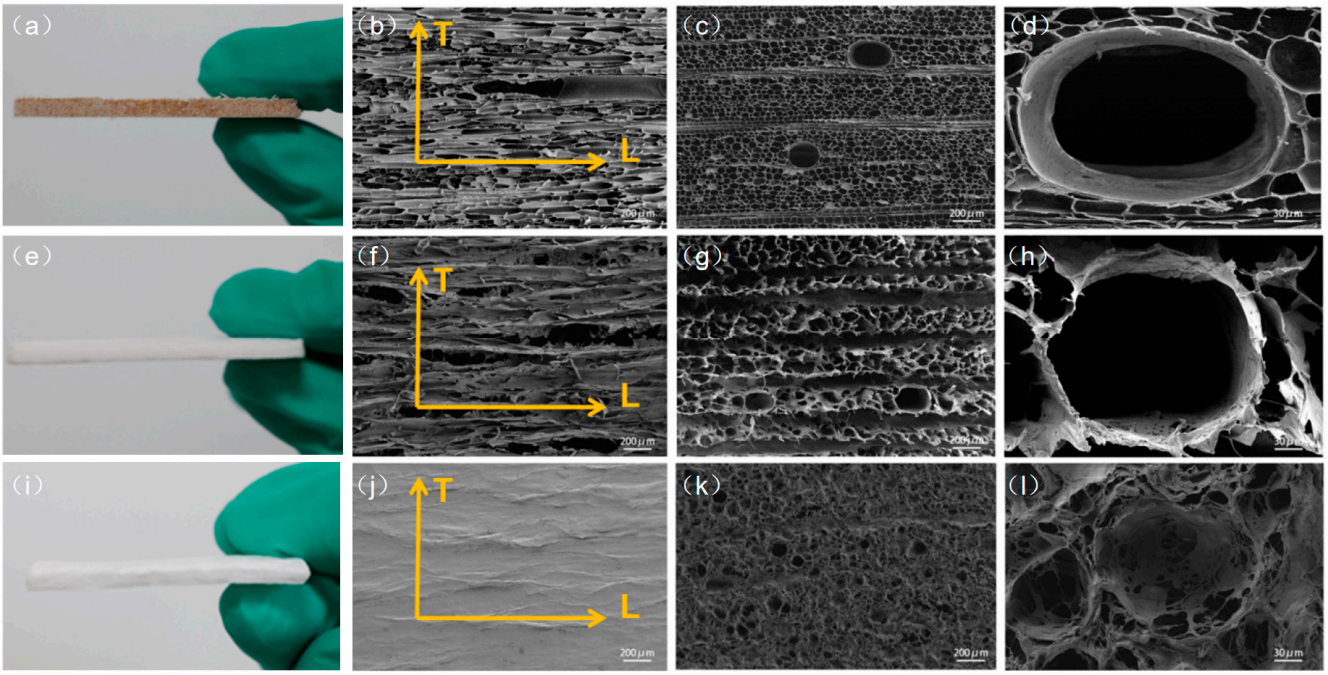

Figure 2. Macroscopic morphology and SEM images of natural wood, delignified wood, and SWE. (**a**,**e**,**i**) Optical photos of natural wood, delignified wood, and SWE. (**b**,**f**,**j**) SEM image of natural wood, delignified wood, and SWE tangential section; (**c**,**g**,**k**) SEM image of natural wood, delignified wood, and SWE cross section; (**d**,**h**,**l**) SEM image of natural wood, delignified wood, and SWE cellular structure.

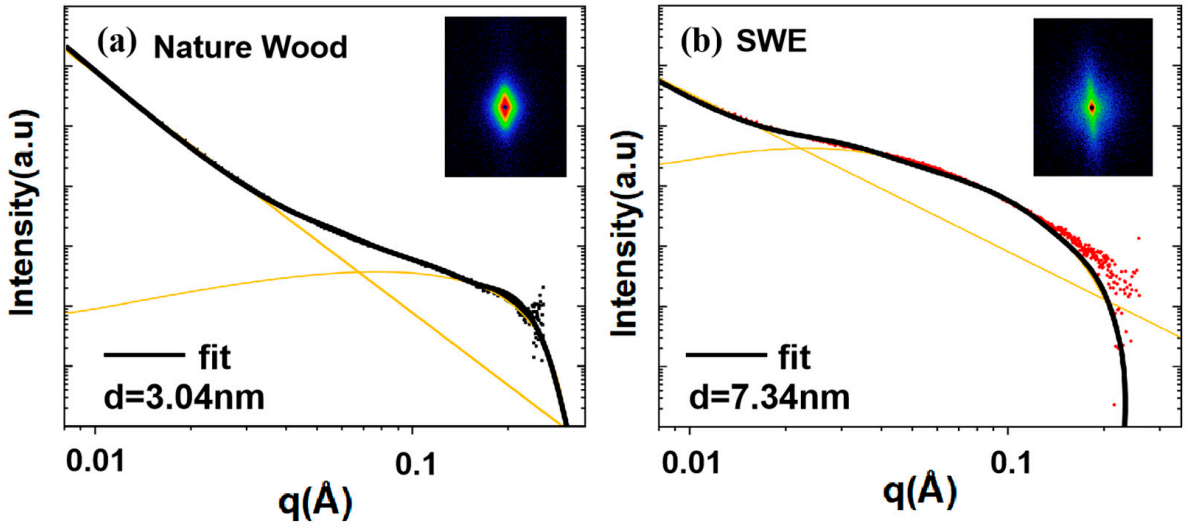

Figure 3. (**a**) 1D and 2D SAXS images of natural wood; (**b**) 1D and 2D SAXS images of SWE.

3.2. The Chemical Properties of SWE

The presence of rigid lignin in wood is an important cause of its elasticity, so the effective removal of lignin is important for the SWE to achieve high elasticity. We tested the contents of the three major elements in virgin and delignified wood (Table 1 and Figure 4). The natural wood contained 33.6% cellulose, 7.3% hemicellulose, and 20.6% lignin. After the delignification treatment, the lignin content decreased from 20.6% to 2.6%, the cellulose content increased from 33.6% to 72.6%, and the hemicellulose content remained almost unchanged, which indicates that this occurred after the NaOH pretreatment as well as $NaClO_2$ (pH ~4.6). This indicates that lignin was mostly removed and that cellulose was retained during the NaOH pretreatment and $NaClO_2$ (pH ~4.6) treatment. The mechanism of lignin removal from wood is that the $NaClO_2$ solution produces ClO_2 during heating, and the phenol radicals in the lignin molecules are oxidized by ClO_2 to form phenoxy radicals. The generated phenoxy radicals further react with ClO_2, and these two successive steps cause the lignin molecules to be converted into muconic acid, or the side chain is broken to form quinone [33].

Table 1. Contents of cellulose, lignin, and hemicellulose in natural wood and delignified wood.

Name	Cellulose (%)	Hemicellulose (%)	Lignin (%)
Nature wood	33.6 ± 0.8	7.3 ± 0.7	20.6 ± 1.7
Delignified wood	72.6 ± 1.2	9.0 ± 0.2	2.6 ± 0.3

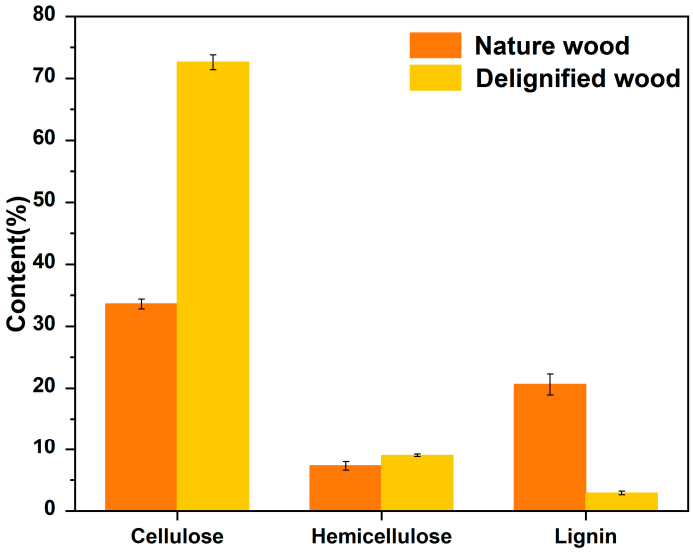

Figure 4. Contents of cellulose, lignin, and hemicellulose in natural wood and delignified wood.

Fourier transform infrared spectroscopy (FTIR) was utilized to further investigate the chemical structure changes of SWE (Figure 5). Compared with the natural wood, the delignified wood showed the absence of peaks of lignin (C-O stretching vibrational absorption peak) at 1232 cm^{-1}, and hemicellulose (non-conjugated C=O vibrational absorption peak) at 1734 cm^{-1} completely disappeared in the delignified wood, indicating that the lignin and hemicellulose in the wood had been completely removed. In the SWE, the absorption peak at 1417 cm^{-1} was attributed to the CH_2 bending vibration of the polyvinyl alcohol molecule, and the absorption peak at 1088 cm^{-1} was attributed to the C-O stretching vibrational mode of the polyvinyl alcohol molecule, which represents the formation of a crosslinked network of PVA molecules with cellulose molecule chains in the SWE.

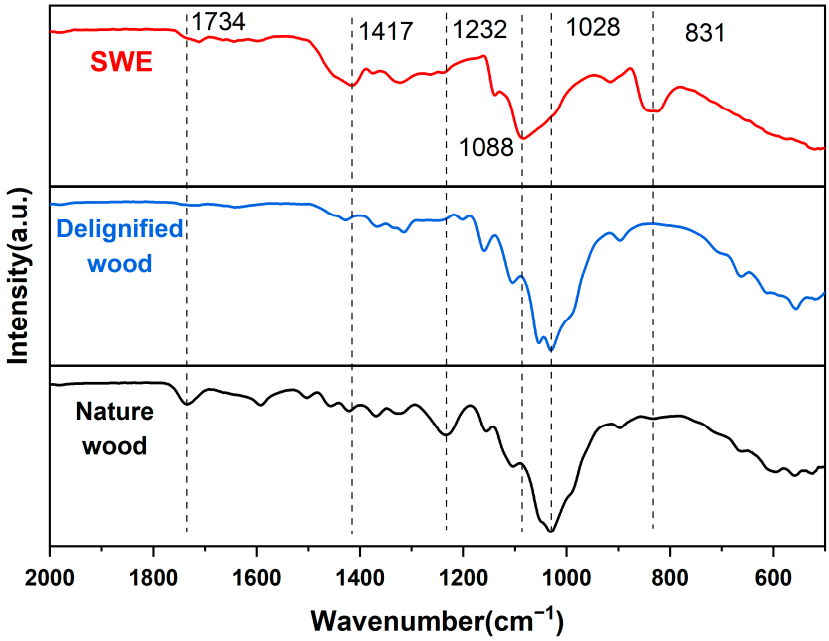

Figure 5. FTIR images of natural wood, delignified wood, and the SWE.

The XRD images indicate that the wood had a typical cellulose I structure, as evidenced by the three characteristic peaks at 34.67°, 21.98°, and 15.35° corresponding to the (040), (002), and (101) lattice planes of cellulose I, respectively (Figure 6). The peaks at the 002 lattice plane reflect the width of the crystalline zone, while the peaks at the 040 lattice plane reflect the length of the crystalline zone. The position of the characteristic peaks after delignification was basically the same as that of the original wood, but the crystallinity increased significantly. This is because amorphous hemicellulose and lignin are selectively removed during delignification, and cellulose is more likely to form a crystal structure through hydrogen bonding interactions. The XRD pattern of SWE retained the I-type structure of cellulose and showed the characteristic peaks of PVA, indicating that PVA molecules were well-filled into the pores of the wood.

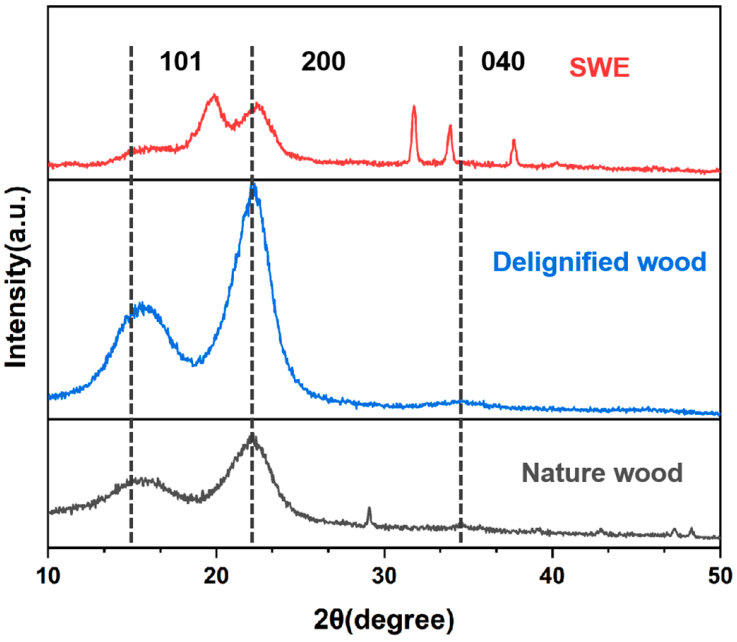

Figure 6. XRD images of natural wood, delignified wood, and the SWE.

3.3. Strengthening and Toughening of SWE

The SWE retained the natural anisotropic structure of wood and exhibited better mechanical properties than virgin wood. We investigated and compared the mechanical properties of the SWE in different directions. In the T direction, the tensile strength of virgin wood was about 2.3 MPa, the strain was about 10%, and the mechanical properties of the SWE were significantly reduced after delignification treatment (Figure 7a,b). The mechanical strength of natural wood in the L direction (~21.3 MPa) was significantly higher than that in the T direction, and the higher mechanical strength was attributed to the oriented arrangement of the cellulose molecular chains. The SWE obtained after reconstitution by PVA impregnation had excellent mechanical properties and the tensile strength increased with increasing PVA concentration. However, the strain of SWE will decrease at higher concentrations (15%PVA), mainly due to the high viscosity and poor fluidity of the high concentration PVA solution, which results in poor permeability in wood (Figure 7a,b). We further improved the mechanical properties of the SWE by using physical freezing and thawing. After eight freeze–thaw cycles, the mechanical properties in the T- and L-directions significantly improved. The mechanical strength in the T-direction increased to 5.63 MPa with a strain of 234% (Figure 7c). Similarly, the tensile strength in the L-direction increased to 25.68 MPa with a strain of 463% (Figure 7f). The freeze–thaw process is comparable to the physical forging of elastomers. During the freezing process, ice crystals repel water molecules from the solvent around them, while dispersing the polymer between them. The ice crystals melt when the temperature rises, releasing the polymers dispersed in them. Due to the interaction forces between the polymers, the polymer molecules are re-crosslinked to form a homogeneous gel structure. By repeating this process, it is possible to continuously squeeze the PVA molecules and cellulose nanofibers against each other to form an entangled network structure [38].

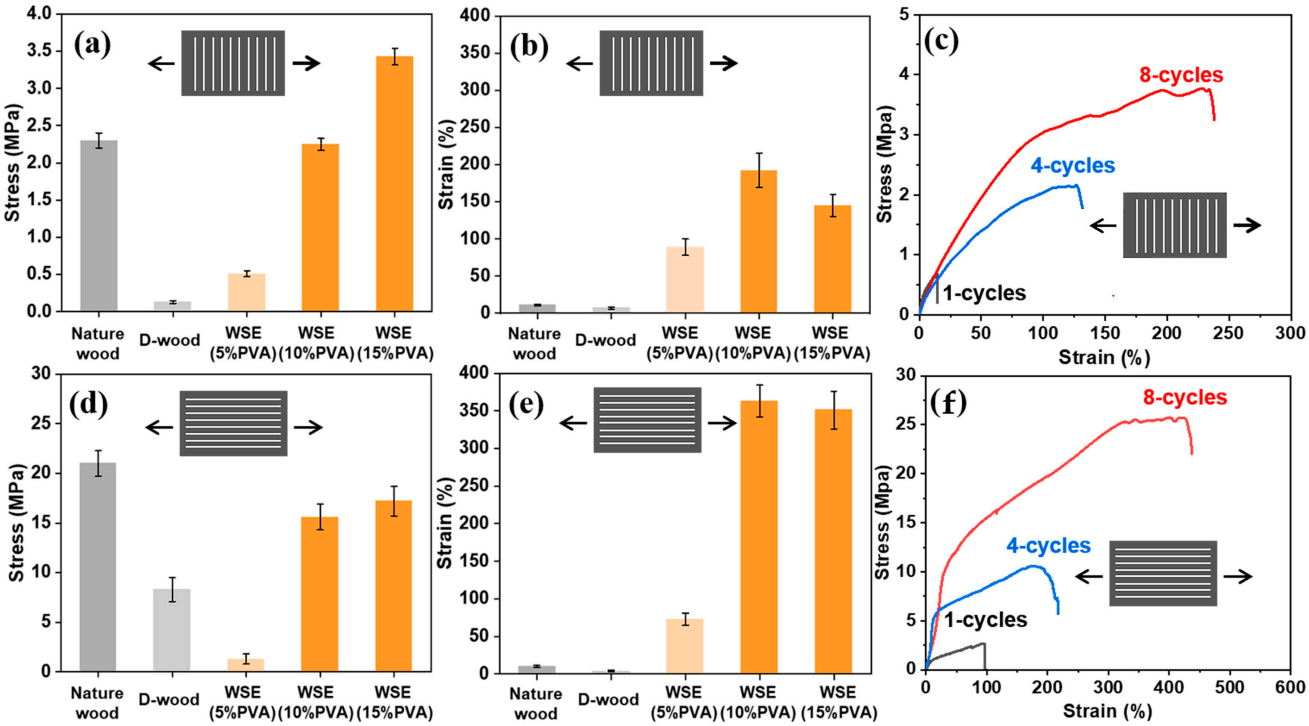

Figure 7. Comparison of the mechanical properties of natural wood, delignified wood, and the SWE (5% PVA, 10% PVA, 15% PVA). (**a**,**b**) Tensile strength and strain of three materials in the T-direction; (**c**) the effect of freeze–thaw cycles on the mechanical properties of the SWE T-direction; (**d**,**e**) the tensile strength and strain of three materials in the L-direction; (**f**) the effect of freeze–thaw cycles on the mechanical properties of the SWE L-direction.

We further used the microscopic in situ stretching technique to observe the micromorphological changes of delignified wood and SWE during stretching in the T-direction (Figure 8). The lignocellulosic fiber backbone was prone to fracture during external stretching (Figure 8a–c), which was related to the weak hydrogen bonding connections between fibers. The PVA in the SWE penetrated into the lignocellulosic fiber backbone and formed a crosslinked network structure, which would mean that it did not fracture during the stretching process (Figure 8e), and that the SWE would return to its original shape when the external force disappeared (Figure 8f).

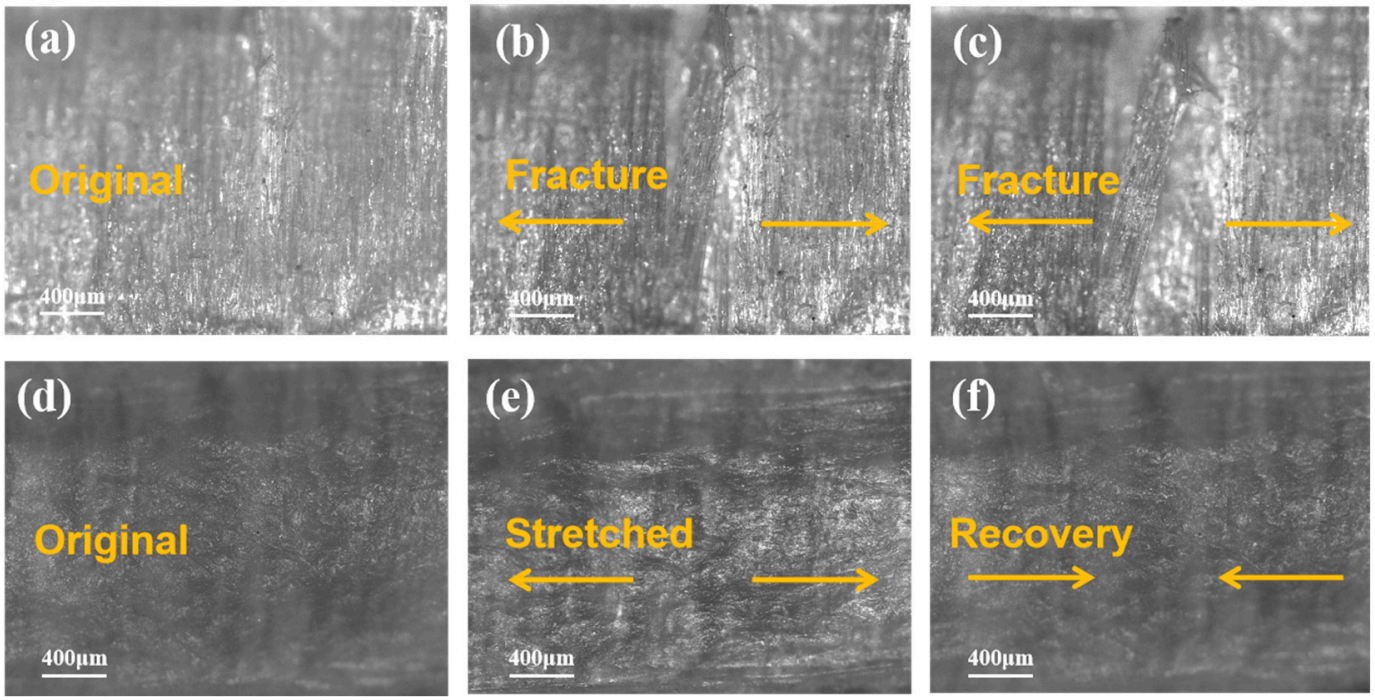

Figure 8. In situ tensile images of delignified light wood and the SWE. (**a**–**c**) Microscopic images of the tensile fracture of delignified wood; (**d**–**f**) microscopic images during the SWE stretching process.

3.4. The Flexible Deformation Capability of SWE

After the delignification and gelation processes, the cellulose fibers in the gel network were cross-linked and entangled with the PVA molecular chains, and the SWE showed a strong flexible deformation ability. Figure 9 shows the digital images of the SWE under different stresses. The basic structure of the SWE was not damaged when it was bent (Figure 9a), and we could also deform the SWE in complex ways such as winding and knotting (Figure 9b). When we stretched the SWE along the T-direction, the SWE showed excellent tensile ability (Figure 9c). Partially open microchannels created space in the SWE (Figure 9d), and the abundant pore channels allowed the SWE to bend and withstand severe deformations without rupturing in order to accommodate various deformations. This unique wrinkled cell wall structure gives the all-wood hydrogel excellent flexibility. The excellent mechanical properties of the SWE can mainly be attributed to the strong hydrogen bonding, physical entanglement, and van der Waals forces between the cellulose nanofibers and the PVA chains as well as the toughening effect of the cellulose nanofibers.

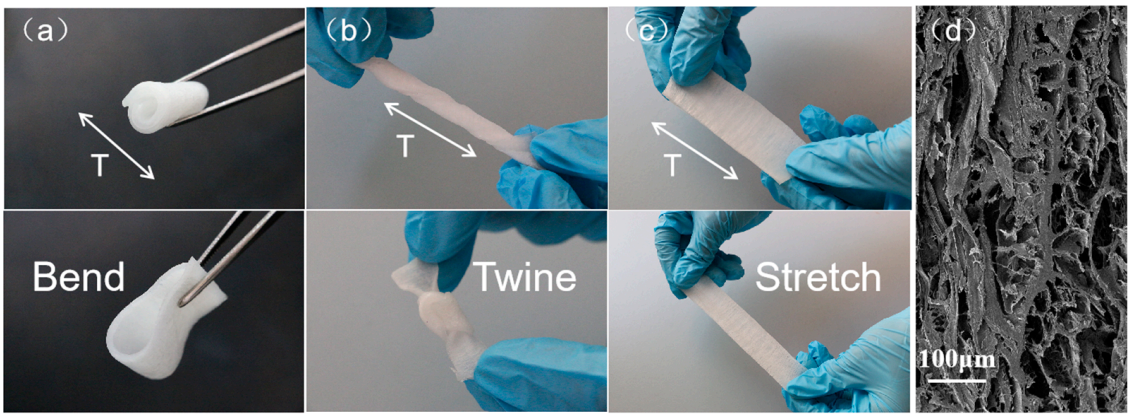

Figure 9. Macro image and micro morphology of the SWE undergoing flexible deformation. (**a**) Bending; (**b**) wrapping and knotting; (**c**) stretching; (**d**) SWE rich pore structure.

3.5. The Application in the Field of Flexible Electronics

In recent reports, cellulose nanofibers in wood are usually used as nanochannels for ion transport. To expand the application area of SWEs, we immersed it in a salt (NaCl) solution for approximately 24 h to allow for sufficient ion permeation. This resulted in the creation of an elastomeric material (E-SWE) with conductive properties. We then connected E-SWE to an electrochemical workstation and recorded the relative resistance change (R/R_0) through repeated stimulation. The well-arranged cellulose nanofibers contain nanochannels that function as fast channels for the ion transport sensor. As shown in Figure 10b, the fluctuation range of the current change value ($(R - R_0)/R_0$) in the L-direction was smaller than that in the T-direction, indicating that the E-SWE has significant anisotropic electro sensitivity.

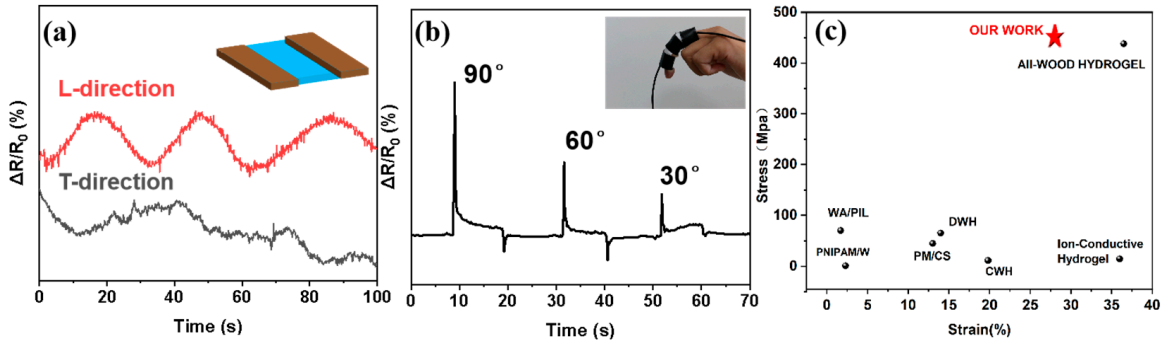

Figure 10. (**a**) Changes in the relative resistance values in the E-SWE L- and T-directions; (**b**) E-SWE detection of finger bending (90°~0°); (**c**) comparison of mechanical properties between SWE and other wood-based elastic materials.

The E-SWE has potential as a sensor for the real-time monitoring of human motions due to its good electrical conductivity, elasticity, and flexibility. As illustrated in Figure 10b, the E-SWE was sensitive enough to monitor the finger flexion at different angles ranging from 90° to ~0°. This suggests that the E-SWE has promising applications in wearable electronic devices. Moreover, in our work, its mechanical properties were superior to the majority of artificial elastomers reported in recent years (Table 2) [24,26,29,39–42]. These include wood-based stretchable elastomers prepared by integrating polymers such as polyacrylamide (PAM), poly(N-isopropylacrylamide) (PNIPAM), and polyvinyl alcohol (PVA) into a delignified wood. It is noteworthy that the all-wood hydrogels and ion-conductive hydrogels also exhibited excellent mechanical properties; however, they inevitably utilize chemical cross-linking in their preparation. In contrast, the SWE formed by physical cross-linking also exhibited mechanical properties that were nearly identical.

Table 2. Comparison of the SWE mechanical performance.

Name	Tensile Strength (MPa)	Strain (%)	Ref.
SWE	28	450	-
WA/PIL	1.7	70	[26]
All-wood hydrogels	36.5	438	[29]
Ion-conductive hydrogels	36	14.5	[39]
DWH	14	65	[40]
PM/CS	13	45	[41]
WCH	19.8	11.3	[24]
PNIPAM/WOOD	2.3	1.1	[42]

4. Conclusions

In conclusion, we synthesized a wood-based elastomeric material with strong mechanical properties by simple physical freeze–thawing without using any chemical cross-linking agent. The prepared SWE exhibited high mechanical strength and high flexibility due to the aligned cellulose as the rigid backbone and PVA as the crosslinking network. The SWE maintained the anisotropic structure of wood and its fiber spacing was significantly increased due to moisture action. The tensile strength in the SWE L-direction after freeze–thaw cycles was 25.68 MPa and the strain was 463%, which were 5 and 2 times higher than those in the T-direction, respectively. In addition, we obtained an E-SWE with sensing properties by immersing it in a salt solution. The E-SWE could detect finger bending in the human body, demonstrating potential applications in wearable electronic devices. Compared to traditional elastomers, the SWE retains the anisotropic structure of wood and has excellent mechanical properties, which makes it more flexible and versatile in its application. Its preparation process is simple, greener, and more economical, and it is a new type of biomass elastomer that has great potential in the field of flexible wearable devices and smart response materials.

Author Contributions: Conceptualization, Y.Z., Y.L. and J.S.; Methodology, J.L.; Validation, J.S.; Formal analysis, Y.Z.; Writing—review and editing, Y.Z. and J.S. All authors have read and agreed to the published version of the manuscript.

Funding: This research was funded by the National Key Research Development Program of China (2023YFD2201405) and the Qing Lan Project to Jiangsu Province (2022).

Data Availability Statement: All data needed to evaluate the conclusions in the paper are presented in the paper. Additional data related to this paper may be requested from the authors.

Conflicts of Interest: The authors declare no conflicts of interest.

References

1. Dakneviciute, V.; Milasiene, D.; Ukvalbergiene, K. Tensile Strength, Elasticity and Cracking Character of Softwood Tissues. *Medžiagotyra* **2015**, *21*, 260–264.
2. Ramage, M.H.; Burridge, H.; Busse-Wicher, M.; Fereday, G.; Reynolds, T.; Shah, D.U.; Wu, G.; Yu, L.; Fleming, P.; Densley-Tingley, D.; et al. The wood from the trees: The use of timber in construction. *Renew. Sustain. Energy Rev.* **2017**, *68*, 333–359. [CrossRef]
3. Shi, X.; Luo, J.; Luo, J.; Li, X.; Han, K.; Li, D.; Cao, X.; Wang, Z.L. Flexible Wood-Based Triboelectric Self-Powered Smart Home System. *ACS Nano* **2022**, *16*, 3341–3350. [CrossRef] [PubMed]
4. Liu, Y.; Lu, C.; Bian, S.; Hu, K.; Zheng, K.; Sun, Q. Reversible photo-responsive smart wood with resistant to extreme weather. *J. Mater. Sci.* **2022**, *57*, 3337–3347. [CrossRef]
5. Ugolev, B.N. Wood as a natural smart material. *Wood Sci. Technol.* **2014**, *48*, 553–568. [CrossRef]
6. Takahashi, A.; Yamamoto, N.; Ooka, Y.; Toyohiro, T. Tensile Examination and Strength Evaluation of Latewood in Japanese Cedar. *Materials* **2022**, *15*, 2347. [CrossRef] [PubMed]
7. Longo, R.; Laux, D.; Pagano, S.; Delaunay, T.; Le Clézio, E.; Arnould, O. Elastic characterization of wood by Resonant Ultrasound Spectroscopy (RUS): A comprehensive study. *Wood Sci. Technol.* **2018**, *52*, 383–402. [CrossRef]
8. Chen, S.; Wu, Z.; Chu, C.; Ni, Y.; Neisiany, R.E.; You, Z. Biodegradable Elastomers and Gels for Elastic Electronics. *Adv. Sci.* **2022**, *9*, 2105146. [CrossRef] [PubMed]
9. Wan, Y.; Li, X.C.; Yuan, H.; Liu, D.; Lai, W.Y. Self-Healing Elastic Electronics: Materials Design, Mechanisms, and Applications. *Adv. Funct. Mater.* **2024**, *early view*. [CrossRef]

10. Walley, S.M.; Rogers, S.J. Is Wood a Material? Taking the Size Effect Seriously. *Materials* **2022**, *15*, 5403. [CrossRef]
11. Keying, L.; Dong, W.; Lanying, L.; Feng, F.U. Research Progress in Multi-scale Interface Structure and Mechanical Properties of Wood. *Trans. China Pulp Pap.* **2021**, *36*, 88–94. [CrossRef]
12. Shumin, Y.; Xing'E, L.; Lili, S.; Jianfeng, M.A.; Genlin, T.; Zehui, J. The Characteristics and Representation Methods of Lignin for Bamboo. *Mater. Rep.* **2020**, *34*, 7177–7182. [CrossRef]
13. Börcsök, Z.; Pásztory, Z. The role of lignin in wood working processes using elevated temperatures: An abbreviated literature survey. *Eur. J. Wood Wood Prod.* **2021**, *79*, 511–526. [CrossRef]
14. Galos, J.; Das, R.; Sutcliffe, M.P.; Mouritz, A.P. Review of balsa core sandwich composite structures. *Mater. Des.* **2022**, *221*, 111013. [CrossRef]
15. Zhang, H.; Zhu, P.; Wang, Z.; Ma, F.; Ji, H.; Li, X. Combined effect of rays and vessels to achieve high strength and toughness in balsa wood. *Mater. Lett.* **2023**, *352*, 135137. [CrossRef]
16. Gao, R.; Huang, Y.; Gan, W.; Xiao, S.; Gao, Y.; Fang, B.; Zhang, X.; Lyu, B.; Huang, R.; Li, J.; et al. Superhydrophobic elastomer with leaf-spring microstructure made from natural wood without any modification chemicals. *Chem. Eng. J.* **2022**, *442*, 136338. [CrossRef]
17. Wang, Z.; Lin, S.; Li, X.; Zou, H.; Zhuo, B.; Ti, P.; Yuan, Q. Optimization and absorption performance of wood sponge. *J. Mater. Sci.* **2021**, *56*, 8479–8496. [CrossRef]
18. Song, D.; Zeng, M.; Min, P.; Jia, X.; Gao, F.; Yu, Z.; Li, X. Electrically conductive and highly compressible anisotropic MXene-wood sponges for multifunctional and integrated wearable devices. *J. Mater. Sci. Technol.* **2023**, *144*, 102–110. [CrossRef]
19. Kuang, X.; Arıcan, M.O.; Zhou, T.; Zhao, X.; Zhang, Y.S. Functional Tough Hydrogels: Design, Processing, and Biomedical Applications. *Acc. Mater. Res.* **2023**, *4*, 101–114. [CrossRef]
20. Li, C.; Wang, C.; Keplinger, C.; Zuo, J.; Jin, L.; Sun, Y.; Zheng, P.; Cao, Y.; Lissel, F.; Linder, C.; et al. A highly stretchable autonomous self-healing elastomer. *Nat. Chem.* **2016**, *8*, 618–624. [CrossRef]
21. Steck, J.; Kim, J.; Yang, J.; Hassan, S.; Suo, Z. Topological adhesion. I. Rapid and strong topohesives. *Extrem. Mech. Lett.* **2020**, *39*, 100803. [CrossRef]
22. Ajdary, R.; Tardy, B.L.; Mattos, B.D.; Bai, L.; Rojas, O.J. Plant Nanomaterials and Inspiration from Nature: Water Interactions and Hierarchically Structured Hydrogels. *Adv. Mater.* **2021**, *33*, e2001085. [CrossRef]
23. Yongyue, Z.; Jiangtao, S.; Zongying, F.; Yun, L. Research Progress of Cellulose Self-Healing Hydrogels. *Sci. Silvae Sin.* **2024**, *60*, 128–138. [CrossRef]
24. Dong, Y.; Pan, N.; Zhu, M.; Tang, M.; Wu, Y.; You, Z.; Zhou, X.; Chen, M. An anti-swelling, strong and flexible wood-based composite hydrogel as strain sensor. *Ind. Crops Prod.* **2022**, *187*, 115491. [CrossRef]
25. Wang, S.; Li, K.; Zhou, Q. High strength and low swelling composite hydrogels from gelatin and delignified wood. *Sci. Rep.* **2020**, *10*, 17842. [CrossRef]
26. Shen, X.; Nie, K.; Zheng, L.; Wang, Z.; Wang, Z.; Li, S.; Jin, C.; Sun, Q. Muscle-inspired capacitive tactile sensors with superior sensitivity in an ultra-wide stress range. *J. Mater. Chem. C Mater. Opt. Electron. Devices* **2020**, *8*, 5913–5922. [CrossRef]
27. Adelnia, H.; Ensandoost, R.; Shebbrin Moonshi, S.; Gavgani, J.N.; Vasafi, E.I.; Ta, H.T. Freeze/thawed polyvinyl alcohol hydrogels: Present, past and future. *Eur. Polym. J.* **2022**, *164*, 110974. [CrossRef]
28. Holloway, J.L.; Lowman, A.M.; Palmese, G.R. The role of crystallization and phase separation in the formation of physically cross-linked PVA hydrogels. *Soft Matter* **2013**, *9*, 826–833. [CrossRef]
29. Yan, G.; He, S.; Chen, G.; Ma, S.; Zeng, A.; Chen, B.; Yang, S.; Tang, X.; Sun, Y.; Xu, F.; et al. Highly Flexible and Broad-Range Mechanically Tunable All-Wood Hydrogels with Nanoscale Channels via the Hofmeister Effect for Human Motion Monitoring. *Nano-Micro Lett.* **2022**, *14*, 84. [CrossRef]
30. Chen, C.; Wang, Y.; Zhou, T.; Wan, Z.; Yang, Q.; Xu, Z.; Li, D.; Jin, Y. Toward Strong and Tough Wood-Based Hydrogels for Sensors. *Biomacromolecules* **2021**, *22*, 5204–5213. [CrossRef]
31. Borrega, M.; Ahvenainen, P.; Serimaa, R.; Gibson, L. Composition and structure of balsa (*Ochroma pyramidale*) wood. *Wood Sci. Technol.* **2015**, *49*, 403–420. [CrossRef]
32. Jung, W.; Savithri, D.; Sharma-Shivappa, R.; Kolar, P. Changes in Lignin Chemistry of Switchgrass due to Delignification by Sodium Hydroxide Pretreatment. *Energies* **2018**, *11*, 376. [CrossRef]
33. Tarvo, V.; Lehtimaa, T.; Kuitunen, S.; Alopaeus, V.; Vuorinen, T.; Aittamaa, J. A Model for Chlorine Dioxide Delignification of Chemical Pulp. *J. Wood Chem. Technol.* **2010**, *30*, 230–268. [CrossRef]
34. Kubo, S.; Kadla, J.F. The Formation of Strong Intermolecular Interactions in Immiscible Blends of Poly(vinyl alcohol) (PVA) and Lignin. *Biomacromolecules* **2003**, *4*, 561–567. [CrossRef] [PubMed]
35. Bian, H.; Wei, L.; Lin, C.; Ma, Q.; Dai, H.; Zhu, J.Y. Lignin-Containing Cellulose Nanofibril-Reinforced Polyvinyl Alcohol Hydrogels. *ACS Sustain. Chem. Eng.* **2018**, *6*, 4821–4828. [CrossRef]
36. Ram, F.; Garemark, J.; Li, Y.; Pettersson, T.; Berglund, L.A. Functionalized Wood Veneers as Vibration Sensors: Exploring Wood Piezoelectricity and Hierarchical Structure Effects. *ACS Nano* **2022**, *16*, 15805–15813. [CrossRef] [PubMed]
37. Chen, P.; Li, Y.; Nishiyama, Y.; Pingali, S.V.; O Neill, H.M.; Zhang, Q.; Berglund, L.A. Small Angle Neutron Scattering Shows Nanoscale PMMA Distribution in Transparent Wood Biocomposites. *Nano Lett.* **2021**, *21*, 2883–2890. [CrossRef] [PubMed]
38. Wu, Y.; Tang, Q.; Yang, F.; Xu, L.; Wang, X.; Zhang, J. Mechanical and thermal properties of rice straw cellulose nanofibrils-enhanced polyvinyl alcohol films using freezing-and-thawing cycle method. *Cellulose* **2019**, *26*, 3193–3204. [CrossRef]

39. Kong, W.; Wang, C.; Jia, C.; Kuang, Y.; Pastel, G.; Chen, C.; Chen, G.; He, S.; Huang, H.; Zhang, J.; et al. Muscle-Inspired Highly Anisotropic, Strong, Ion-Conductive Hydrogels. *Adv. Mater.* **2018**, *30*, 1801934. [CrossRef]
40. Zhang, R.; Wu, C.; Yang, W.; Yao, C.; Jing, Y.; Yu, N.; Su, S.; Mahmud, S.; Zhang, X.; Zhu, J. Design of delignified wood-based high-performance composite hydrogel electrolyte with double crosslinking of sodium alginate and PAM for flexible supercapacitors. *Ind. Crops Prod.* **2024**, *210*, 118187. [CrossRef]
41. Wang, Z.; Zhou, Z.; Wang, S.; Yao, X.; Han, X.; Cao, W.; Pu, J. An anti-freezing and strong wood-derived hydrogel for high-performance electronic skin and wearable sensing. *Compos. Part B Eng.* **2022**, *239*, 109954. [CrossRef]
42. Chen, L.; Wei, X.; Wang, F.; Jian, S.; Yang, W.; Ma, C.; Duan, G.; Jiang, S. In-situ polymerization for mechanical strong composite actuators based on anisotropic wood and thermoresponsive polymer. *Chin. Chem. Lett.* **2022**, *33*, 2635–2638. [CrossRef]